Energy & Environmental Science

PAPER

Quantifying and Elucidating the effect of CO_2 on the Thermodynamics, Kinetics and Charge Transport of AEMFCs

Received 00th January 20xx,
Accepted 00th January 20xx

DOI: 10.1039/x0xx00000x

Yiwei Zheng,[a] Travis J. Omasta,[a] Xiong Peng,[a] Lianqin Wang,[b] John R. Varcoe,[b] Bryan S. Pivovar[c] and William E. Mustain[a*]

It has been long-recognized that carbonation of anion exchange membrane fuel cells (AEMFCs) would be an important practical barrier for their implementation in applications that use ambient air containing atmospheric CO_2. Most literature discussion around AEMFC carbonation has hypothesized: 1) that the effect of carbonation is limited to an increase in the Ohmic resistance because carbonate has lower mobility than hydroxide; and/or 2) that the so-called "self-purging" mechanism could effectively decarbonate the cell and eliminate CO_2-related voltage losses during operation at a reasonable operating current density (> 1 A cm^{-2}). However, this study definitively shows that neither of these assertions are correct. This work, the first experimental examination of its kind, studies the dynamics of cell carbonation and its effect on AEMFC performance over a wide range of operating currents (0.2 – 2.0 A cm^{-2}), operating temperatures (60 – 80°C) and CO_2 concentrations in the reactant gases (5 – 3200 ppm). The resulting data provides for new fundamental relationships to be developed and for the root causes of increased polarization in the presence of CO_2 to be quantitatively probed and deconvoluted into Ohmic, Nernstian and charge transfer components, with the Nernstian and charge transfer components controlling the cell behavior under conditions of practical interest.

Broader context

Anion exchange membrane fuel cells (AEMFCs) have shown significant promise to provide clean, sustainable energy for grid and transportation applications – and at a lower theoretical cost than more established proton exchange membrane fuel cells (PEMFCs). Adding to the excitement around AEMFCs is the extremely high peak power that can now be obtained (> 3 W cm^{-2}) and continuously improving durability (1000+ h), which has made the future deployment of AEMFCs in real-world applications a serious consideration. For some applications (*e.g.* automotive), the most critical remaining practical issue with AEMFCs is understanding and mitigating the effects of atmospheric CO_2 (in the air supply) on cell behavior and performance. This study is the first comprehensive experimental investigation into the effects of CO_2 on operating AEMFCs. It is also the first study to be able to quantitatively determine the root causes for performance decline when CO_2 is added to the system, where cell behavior is directly linked to cell chemistry and reaction dynamics. In addition to the demonstrated technology, the lessons learned in this work can also provide transformational insights to other air breathing and/or AEM-based electrochemical systems such as metal air batteries, regenerative fuel cells, electrochemical CO_2 capture, CO_2 reduction reactors and dialyzers.

Introduction

For decades, the proton exchange membrane fuel cell (PEMFC) has dominated the research space for low temperature polymer electrolyte fuel cells. Though significant advances have been made regarding the performance and stability of PEMFCs over the years, one of the factors that has limited its wide deployment is cost [1]. It has been broadly suggested in recent years that a change of electrolyte to a solid alkaline polymer electrolyte might be able to significantly reduce the cost of polymer-based fuel cell systems [2] because the alkaline environment would allow for the deployment of a broader range of noble metal free catalysts as well as less expensive materials to be used for other cell components such as the membrane and bipolar plates.

Early development of these so-called anion exchange membrane fuel cells (AEMFCs) was hindered by anion exchange membranes (AEMs) with very poor alkaline stability [3] and very poor performance, with typical peak power densities well below 0.5 W cm^{-2}. The combination of low achievable power and limited durability [4,5] made AEMFCs uncompetitive with PEMFCs for years. However, over the past two years, a significant increase in the peak power density has been observed [5–9], with state-of-the-art AEMFCs having the ability to achieve values over 3 W cm^{-2} operating on H_2/O_2 gas feeds[10]. Also, the performance stability of AEMFCs has improved dramatically during this time, with multiple groups reporting 500+ hour stability at low degradation rates (5 – 10%) [11–14].

Now that AEMFC performance and stability has been enhanced to the point where their future deployment in real applications can be seriously contemplated, it is now an important time in AEMFC development to begin to answer

[a] *Department of Chemical Engineering, University of South Carolina, Columbia, South Carolina 29208, USA. E-mail: mustainw@mailbox.sc.edu*
[b] *National Renewable Energy Laboratory, Golden, Colorado 80401, USA.*
[c] *Department of Chemistry, University of Surrey, Guildford, GU2 7XH, UK.*
† Electronic Supplementary Information (ESI) available: Figures S1 – S9, Table S1-S4, experimental details and additional analysis. See DOI: 10.1039/x0xx00000x

some of the other lingering issues that have to date been mostly put aside in the literature. It can be argued that one of the most important of these issues is understanding and mitigating the effects of atmospheric CO_2 on AEMFC performance. It is widely known that when CO_2-containing air is fed to the AEMFC cathode, the OH^- anions that are produced from the oxygen reduction reaction (ORR), Equation 1, react with CO_2 to produce carbonate and/or bicarbonate anions, Equations 2-3.

$$O_2 + 2H_2O + 4e^- \rightarrow 4OH^- \quad (1)$$
$$CO_2 + OH^- \rightleftharpoons HCO_3^- \quad (2)$$
$$HCO_3^- + OH^- \rightleftharpoons CO_3^{2-} + H_2O \quad (3)$$

As (bi)carbonate anions are produced, they are transported towards the anode by migration, resulting in a "carbonation" of the anion exchange membrane (AEM) as well as the ionomer in the electrodes (especially the anode). This carbonation results in a severe reduction in the operating cell voltage, with carbonate-related overpotentials as high as 400 mV [15]. Though theoretical studies have tried to shed some light on this phenomena [16,17], unfortunately, there is a very small body of experimental work in the literature quantifying the impact of CO_2 and determining the root causes behind the extensive performance drop for AEMFCs when CO_2 is present.

Therefore, the purpose of this study is to establish a resolute understanding of the influence of CO_2 on the performance of AEMFCs. Herein, the CO_2 concentration in both the cathode and anode are parametrically changed over a wide range of conditions (current density and temperature) that represent reasonable ranges for their practical operation. Finally, this work explores the lower limits of CO_2 exposure to determine whether or not there is a baseline CO_2 tolerance in AEMFCs, which informs the field to what degree oxidant gas scrubbing might be needed.

Experimental

Electrode Preparation

The electrodes in this work were prepared using a method that has been detailed in our previous publications [8,9]. Briefly, the anode and cathode catalysts were 60 wt% PtRu supported on Vulcan XC-72R (Alfa Aesar HiSPEC 10000, 2:1 ratio of Pt:Ru by mass – Pt nominally 40 wt%, and Ru, nominally 20 wt%) and 40 wt% Pt supported on Vulcan XC-72R (Alfa Aesar HiSPEC 4000, Pt nominally 40 wt%), respectively. Electrode preparation was initiated by placing an ethylene tetrafluoroethylene (ETFE) benzyltrimethylammonium (BTMA) solid powder anion exchange ionomer (AEI) with an ion-exchange capacity (IEC) of 1.24 mmol g^{-1} [18] into a mortar and manually grinding it with a pestle for 10 min. The catalyst powder, additional Vulcan carbon (XC-72R, Cabot), and 1 mL of Millipore deionized (DI) water (18.2 MΩ cm resistivity) were added to the mortar and ground for 10 min. The mass fraction of AEI in the catalyst layer was always 0.20 and the total mass fraction of carbon was maintained at 0.48 for both electrodes. Next, the catalyst-AEI slurry was transferred to a polypropylene vial. Isopropyl alcohol was added, and the mixture was sonicated (Fisher Scientific FS30H) for 60 min. The water in the ultrasonic bath was maintained below 5 °C to avoid degrading the supported catalyst and the AEI and to maximize the electrochemically active area by avoiding agglomeration. The ink dispersions were sprayed onto Toray TGP-H-0600 gas diffusion layers with 5% PTFE wetproofing with an Iwata Eclipse HP-CS (feed gas was 15 psig Ultra High Purity N_2) to create gas diffusion electrodes (GDEs). The target GDE catalyst loading was 0.6 ± 0.1 mg_{Pt} cm^{-2}.

Anion Exchange Membrane Fuel Cell (AEMFC) Assembly and Break-in Procedure

Before cell assembly, the GDEs were soaked in 1 M aqueous KOH solutions (prepared from Fisher Chemical pellets/certified ACS and DI water) for 60 min, exchanging the solution twice during this time. At the same time, the AEM was also soaked in an identical solution. Two different AEMs were used in this work. The first was a 50 µm thickness (fully swollen in water) ETFE-BTMA radiation-grafted AEM [19], which was used for the CO_2 dosing experiments at 60 °C. The second AEM was a 25 µm thickness (fully swollen in water) LDPE(low density polyethylene)-BTMA radiation-grafted AEM [7]. The LDPE-BTMA AEM is more chemically and mechanically stable at elevated temperatures than its ETFE-BTMA counterpart and was used when investigating the influence of elevated temperature on CO_2-related overpotential losses.

After soaking for 1 h, excess KOH was removed from the GDEs and AEMs before cell assembly. The GDEs and AEMs were pressed together in the cell to form the membrane electrode assembly (MEA) with no prior hot pressing. The MEAs were loaded into 5 cm^2 Scribner hardware between two single pass serpentine graphite flow plates. An 850e Scribner Fuel Cell Test Station was used to control the gas stream dew points, cell temperature, gas flowrates and the operating current density.

Before CO_2 measurements were made, all cells underwent a break in procedure. First, the cell was brought to its operating temperature under N_2 flow on both sides of the cell at 100% relative humidity. Next, the feed gases were switched to Ultra High Purity H_2 and O_2 (Airgas) at the anode and cathode, respectively. Then, the cell was operated galvanostatically stepwise from 0.7 V to 0.3 V (0.1 V steps, held for a minimum of 30 min at each step) as the reacting gas dew points were optimized per our standard procedure [8]. The optimized reacting gas dew points were very repeatable from cell-to-cell; the dew points were typically 52°C at the anode and 54°C at the cathode for an AEMFC operating at 60°C. Following the optimization of the reacting gas dew points, the cells were operated galvanostatically at the current density of interest (0.2, 0.5, 1.0 or 2.0 A cm^{-2}) and allowed to equilibrate for at least 30 min before CO_2 exposure was initiated. Multiple cells (no less than three) were constructed and tested for each measurement.

AEMFC Carbon Dioxide Measurements

Following the break-in procedure and 30 min equilibration, the cell current was maintained and CO_2 was parametrically added to the Ultra High Purity O_2 cathode stream. We chose to add CO_2

to O_2 instead of air in order to simplify observations and isolate the effects of CO_2 on performance, since air has additional O_2 mass transport impact (*e.g.* N_2 dilution) during cell operation, which is largely eliminated by utilizing O_2 as the reacting gas. The flowrate for O_2 and H_2 in all experiments was 1 L min^{-1}. CO_2 cathode concentrations as low as 2 ppm and as high as 3200 ppm were tested. Typically, after CO_2 addition, the cell was operated for 30 min, which was much longer than the time required to reach quasi-steady-state operation (typically < 5 min, though lower CO_2 concentrations took longer). After 30 min operation at constant current, CO_2 was removed from the gas stream and the cell was allowed to decarbonate for an initial 30 min. After this, the cell was further decarbonated through self-purging by one of two approaches: i) the cell was allowed to operate at the same current density until the voltage reached its pre-CO_2 level and no CO_2 emission was measured at the anode (shown in Figure S1 in the Supporting Information file); or ii) more typically, to reduce the time between CO_2 trials, the cell potential was pulsed down to 0.1 V for 1 min (Figure S2 in the Supporting Information file), after which no CO_2 emission was measured in the anode stream. When CO_2 was fed to the cathode, the concentration of CO_2 being emitted from the anode and cathode were both constantly monitored in real time using a PP Systems WMA-5 non-dispersive infrared CO_2 gas analyzer (a water trap was placed in-line before the WMA-5 in order to preserve the unit and its calibration).

A second set of experiments were done where CO_2 at concentrations between 2 and 400 ppm were added to the anode instead of the cathode. This was meant to simulate two possible scenarios: i) CO_2 accumulation in the anode; and ii) CO_2 exposure at the anode from the oxidation of carbonaceous fuels (through reforming or direct alcohol oxidation). When CO_2 was fed to the anode, the concentration of CO_2 being emitted from the anode and cathode was constantly monitored in real time using the WMA-5. The cathode data will not be shown since the CO_2 concentration there was always below the detection limit during operation (though a very small amount of CO_2 was observed in the cathode exhaust when the cell current was turned off due to diffusion across the AEM, which is shown).

The final set of experiments investigated the effects of temperature on CO_2-related voltage losses. CO_2 was fed separately to both the cathode and anode at 400 ppm. The cell setup and operation were identical to the previous description with one exception: the AEM used for these temperature studies was LDPE-BTMA (IEC = 2.5 mmol g^{-1}), and not ETFE-BTMA (IEC = 2.05 ± 0.05 mmol g^{-1}), because of its superior thermomechanical stability.

Results and discussion

In a typical analysis of fuel cell performance, it is often assumed that the cell voltage (V_{cell}) can be represented by Equation 4:

$$V_{cell} = V_{OCV} - i(R_{\Omega,} + R_{ct} + R_{mt}) \quad (4)$$

where V_{OCV} is the open-circuit voltage, i is the cell current, R_{Ω} is the Ohmic resistance to ion transport, R_{ct} is the charge transfer resistance and R_{mt} is the mass transport resistance. In PEMFCs, it is typically assumed that R_{ct} is dominated by the oxygen reduction reaction (ORR), but this is likely a poor assumption in AEMFCs where the kinetics for the hydrogen oxidation reaction (HOR) are slower in alkaline *vs.* acid electrolyte and the HOR overpotential can be significant [20]. Therefore, discussion regarding charge transfer resistance should take into consideration both the ORR and HOR, which can be denoted as R_{ctORR} and R_{ctHOR}, respectively. PEMFCs also assume that R_{mt} is dominated by oxygen diffusion, which is likely to hold in AEMFCs as well (can be denoted as R_{mtORR}), though this can often be neglected with high stoichiometry pure O_2 flows). However, the presence of CO_2 and carbonate anions complicates this type of analysis.

The electrochemical production of hydroxide anions in the presence of CO_2 and their subsequent equilibrium reactions were summarized in Equations 1 – 3. It should be noted here that $OH^-/CO_3^{2-}/HCO_3^-$ equilibrium constants exist such that OH^- and HCO_3^- can never exist together in large quantities. However, CO_3^{2-} can exist in high concentrations with either OH^- or HCO_3^-. During cell operation at practical current densities, a significant amount of OH^- is produced and CO_2 is purged from the cell. Therefore, the two ions that dominate under operating conditions are OH^- and CO_3^{2-}, which has been confirmed through theoretical modeling [16]. For this reason, the remainder of the discussion in this work will only consider the presence of "carbonate" as CO_3^{2-}, although it is recognized that bicarbonate is often present in highly carbonated AEMs and AEMFCs before significant levels of electrochemical ORR have occurred at the cathode. It is also possible for there to be at least some bicarbonate accumulated in the anode if the degree of carbonation in the AEMFC is high.

After their formation at the cathode, the CO_3^{2-} anions are transported through the AEM to the anode by migration, resulting in the "carbonation" of the AEM and the catalyst layer ionomers (Figure 1). This carbonation reduces the AEM conductivity since CO_3^{2-} has a lower intrinsic mobility than OH^- [21–23], which increases the area-specific resistance (ASR, estimated as the product of the measured high frequency resistance and the cell active area) relative to OH^--only operation (ΔASR). However, this effect should not be overstated as it is only able to account for a small fraction of the performance loss when CO_2 is added to the cathode stream. Definitive experimental evidence will be presented below to support this. Less discussed, though thoughtfully pointed out and modeled by a few studies in the literature[16,24,25], migration is not the only mass transport event that influences the location and distribution of CO_3^{2-}; diffusion also plays a role. The interplay between migration and diffusion results in carbonate concentration profiles that impact performance in two primary ways beyond Ohmic considerations, one pH-based (Nernstian) and the other electrocatalytic[26]

The first CO_2-related effect is pH related and due to a concentration gradient, that builds up across the cell. Under typical operating currents, net migration of ions across the AEM is very fast (on the order of 1 s at relevant current densities and AEM thicknesses). This ionic flux towards the anode leads to

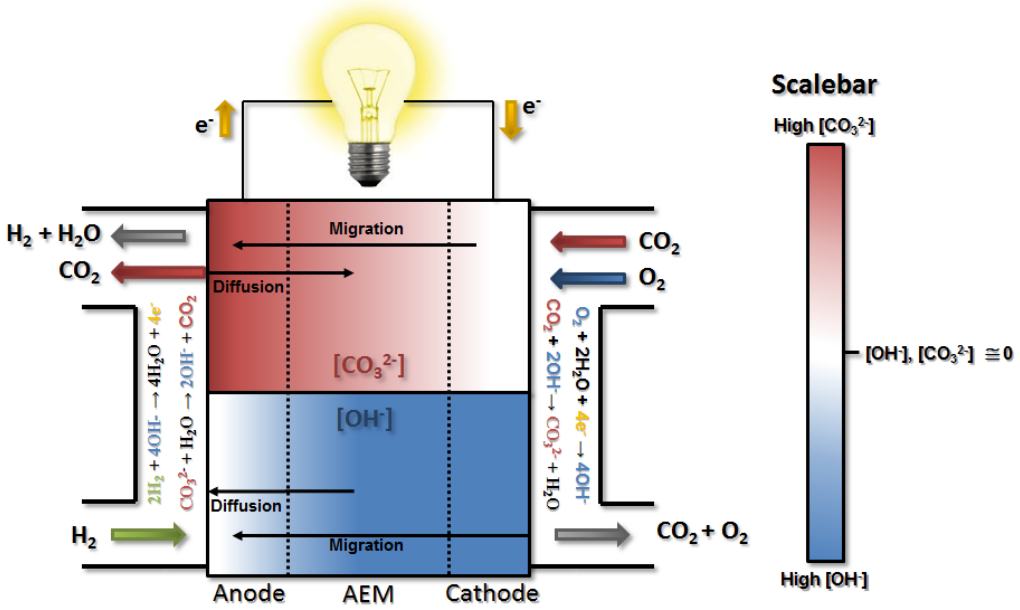

Figure 1. Illustration of the carbonate and hydroxide transport and distribution in operating AEMFCs with CO_2 present in the cathode reacting gas. The top section of the diagram isolates the CO_3^{2-} behavior in operating cells, with the color gradient representing the concentration gradient. The top section of the diagram shows the OH^- concentration gradient, as well as the directionality for hydroxide migration and diffusion.

lower concentrations of CO_3^{2-} in the AEM and cathode compared to the anode (though the extent will depend on factors including membrane thickness, current density and the CO_2 concentration in the cathode stream). The resulting CO_3^{2-} concentration gradient provides a driving force for back-diffusion of CO_3^{2-} anions from the anode towards the cathode – setting up a steady-state concentration gradient where there is significant carbonate accumulation within the anode [16,24,26], although the absolute and variation of the carbonate level within the anode has yet to be determined directly. The presence of carbonate in the anode decreases the local pH, leading to an increase in the anode potential (ΔV_{Nernst}) according to the Nernst equation during operation, which has been theoretically estimated to be as high as 180 – 350 mV [16,27].

The second effect arises from the reduced migrational supply and reduced local concentration of reacting OH^- anions as CO_3^{2-} carries charge from the cathode to the anode and accumulates there. Previous work (and the data in Figure S2 in the Supporting Information for cell pulsing to 0.1 V) has shown evidence that at high anode overpotentials that CO_2 is quickly removed from operating AEMFCs – suggesting that carbonate may directly react with H_2 at those overpotentials to produce water and CO_2, thereby significantly accelerating decarbonization (also supported by data on slide 17 in Ref. [28]). However, the long timescales needed to completely decarbonate AEMFCs at typical operating current and higher cell voltages (lower anode overpotentials), such as Figure S1 in the Supporting Information, strongly suggests that such direct reaction does not appreciably occur at conditions of practical interest. Hence, it can be assumed in this work that essentially the entirety of the steady-state electrochemical current is generated through OH^--based ORR and HOR reactions (Equations 1 and 5, respectively). Therefore, when CO_3^2 anions carry charge through the AEM, the balance of reacting OH^- that is no longer supplied by migration (due to CO_3^{2-} conduction) must be compensated for by diffusion, which is an intrinsically slower process.

$$H_2 + 2OH^- = H_2O + 2e^- \quad (5)$$

Therefore, CO_3^{2-} in the anode effectively shuts off catalyst sites with high local CO_3^{2-} concentration due to reduced access to OH^- ions – increasing the effective current density on OH^- accessible anode catalysts. This means that although the presence of carbonate species does not negatively impact the intrinsic HOR electrocatalysis [29], the high CO_3^{2-} concentration in the anode does cause an increase in the kinetic resistance, inducing polarization losses that lower the operating cell voltage (denoted as ΔR_{ctHOR}).

These new resistances lead to a more complex equation for the operating cell voltage, though one that is insightful for the analysis of AEMFCs that have been carbonated:

$$V_{cell} = V_{OCV} - i\left(R_{\Omega,OH} + R_{ctORR} + R_{mtORR} + R_{ctHOR}\right) - \Delta V_{Nernst} - i(\Delta ASR + \Delta R_{ctHOR}) \quad (6)$$

The assignment of all of the new kinetic overpotential to the anode is supported by experimental work by Matsui *et al.* [30] who found, using a three-electrode AEMFC configuration with a reversible hydrogen reference electrode, that the cathode overpotential was hardly changed by the presence of CO_2, while the overpotential of the anode increased considerably.

The above-discussed behavior of carbonated AEMFCs is very similar to cation-contaminated PEMFCs [31–34], though some critical differences do exist. Most importantly, in this case the "contaminant", CO_3^{2-}, is continuously created at the cathode,

moved to the anode, and removed from the anode gas stream. Similar processes do not exist for cation-contaminated PEMFCs with the exception of the NH_3/NH_4^+ couple [35]. For CO_2 containing AEMFCs, CO_3^{2-} can be removed during operation by introducing a CO_2-free oxidant, activating a "self-purging" mechanism, which has been discussed elsewhere [15]. For reasons discussed above, under normal operating conditions this self-purging is not a result of direct electrochemical reaction of carbonates, but rather thermodynamic equilibrium. Under pseudo steady-state conditions, the CO_2 uptake rates at the cathode equal the release rates at the anode and a static concentration polarization exists across the anode, AEM, and cathode – based on balancing between migration and diffusion of OH^- and CO_3^{2-}, as illustrated in Figure 1.

In order to minimize the effect of CO_2 and carbonation on operating AEMFCs, it is important for the field to better understand how CO_2 uptake, membrane carbonation, and CO_2 release occur. There are both transient and steady-state concerns with little experimental data to provide insight or validate existing models. The results presented here quantify the uptake and release rates of CO_2, quantify the amount of CO_2 within the MEA under different steady-state conditions, and provide data as to the performance and resistance of AEMFCs under specific CO_2 conditions. This first of its kind data provides significant insight into the performance losses and ultimate potential of AEMFCs when exposed to CO_2. This work provides direct evidence regarding the extent to which the CO_2 fed to the cathode becomes integrated into the AEMFC, directly correlates carbonation with AEMFC performance, and provides critical data needed to validate modeling efforts that try to quantify rates of CO_2 uptake and release.

Dynamic Observation of CO_2 Uptake and Transport in Operating AEMFCs

To probe the uptake and release of CO_2 in AEMFCs, CO_2 (100, 200, 400, 800, 1600 and 3200 ppm) was added to the cathode of cells under open circuit conditions as well as cells operated at 0.2, 0.5, 1.0 and 2.0 A cm^{-2}. For the entire data set, the concentration of CO_2 leaving both the anode and cathode was measured in real time. The results for 400 ppm CO_2 in O_2 are shown in Figures 2a and 2b, and the results for all of the other CO_2 concentrations are shown in the Supporting Information file, Figures S3-S7. The first condition assessed was steady-state at the open-circuit voltage (OCV, labeled as 0.0 A cm^{-2}), which allows the diffusional dynamics of ionomer and membrane carbonation to be observed since there is no current driving the movement of CO_3^{2-} from the cathode to the anode. Though the OCV did not change, in agreement with the work by Inaba *et al.* [36], it was clear during the experiment that the AEM and AEI were being converted to the carbonate form since the amount of CO_2 leaving the cathode was far below the 400 ppm feed, Figure 2b, especially over the first 300 s.

After the CO_2 was added to the cathode at OCV, the concentration initially rose from zero to *ca.* 130 ppm as two things were occurring: absorption of CO_2 into the AEM and ionomer and the increase in the CO_2 partial pressure in the gas stream (the humidifier and cell lag in the CO_2 concentration is denoted as "blank" in Figure 2b - determined in a cell containing a Teflon membrane, which does not uptake CO_2 and form CO_3^{2-} anions). Comparing the "blank" and 0.0 A cm^{-2} (black dotted line) plots in Figure 2b, it was clear that there was rapid CO_2 uptake into the AEM because the concentration of CO_2 leaving the AEM-containing cell was always lower than the "blank". By 600 s, the concentration of CO_2 in the cathode rose to the inlet concentration, suggesting that the AEM was extensively

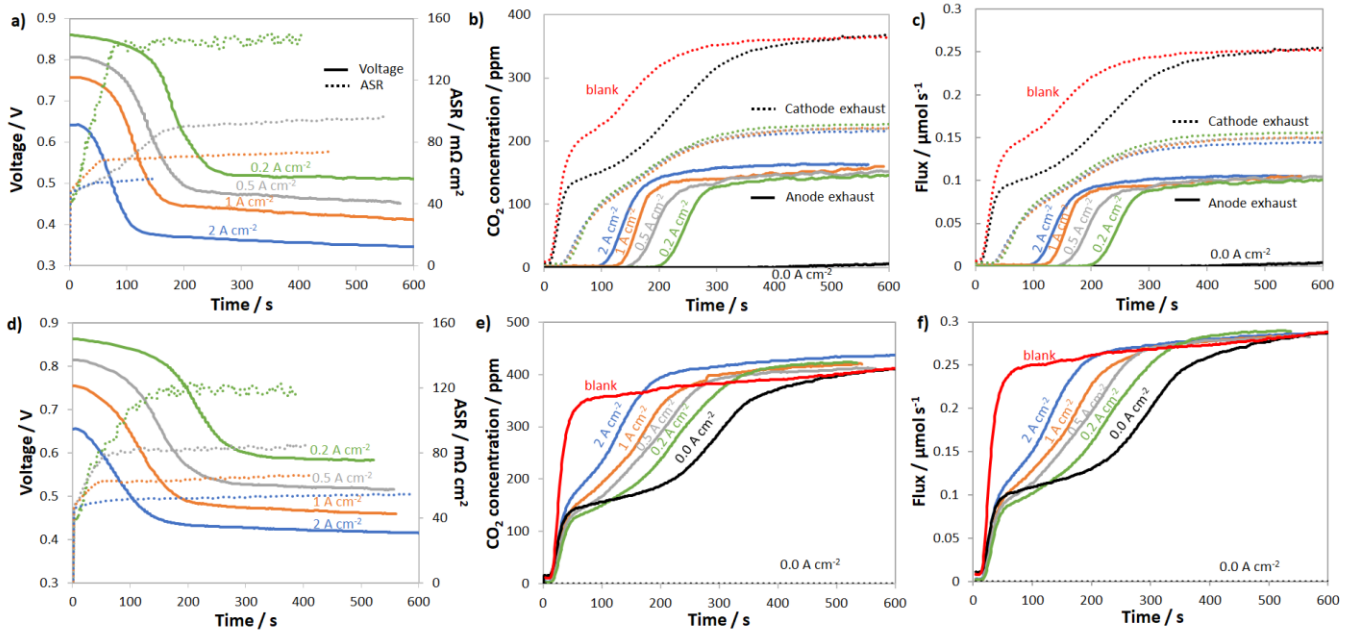

Fig. 2. Uptake of 400 ppm CO_2 fed to both the anode and cathode of H_2/O_2 AEMFCs operating at 60°C and discharging at 0.00 (load off), 0.20, 0.50, 1.0 and 2.0 A cm^{-2} current densities. a) voltage decrease and ASR increase upon introduction of CO_2 into the cathode reacting gas; b) CO_2 emission from the anode (solid lines) and cathode (dotted lines) when 400 ppm CO_2 was fed to the cathode; c) CO_2 flux fed to the cell and released from the anode (solid lines) and cathode (dotted lines) when 400 ppm CO_2 was fed to the cathode; d) voltage decrease and ASR increase upon introduction of CO_2 into the anode reacting gas; e) CO_2 emission from the anode (solid lines) and cathode (dashed line) when 400 ppm CO_2 was fed to the anode; f) CO_2 molar flux fed to the cell and released from the anode (solid lines) and cathode (dashed line) when 400 ppm CO_2 was fed to the anode. The AEM used was ETFE-BTMA (IEC = 2.05 mmol g^{-1}).

carbonated after 10 min, which is in good agreement with previous studies on AEM carbonation in the presence of gas-phase CO_2 [15,37,38]. Also from the difference in the response of the AEM and "blank", it was possible to calculate that essentially all of the charge carrying groups in the AEM and AEI were carbonated during this time (and at steady-state contained a mixture of HCO_3^- and CO_3^{2-}, details in the Supporting Information file, Figure S8 and accompanying discussion).

When CO_2 was added to the cathode of a fully broken-in cell operating at a constant current density, the cell response was very different. In all cases (from 0.2 A cm^{-2} to 2.0 A cm^{-2}), after a brief time lag, the cell operating voltage precipitously declined, the ASR increased, and CO_2 was emitted at the anode; this is shown in Figures 2a and 2b. What changed with current density were the magnitude and timing of these phenomena. At the highest current density that was tested, 2.0 A cm^{-2}, it took approximately 31 s for CO_2 to be measured in the anode stream (from the time that the reacting gas CO_2 concentration increased). It took another 96 s after CO_2 was initially measured in the anode gas before a quasi-steady-state was achieved. When the current was halved to 1.0 A cm^{-2}, the time for CO_2 break-through to the anode was approximately doubled (65 *vs.* 31 s), though the time to reach equilibration was very similar (90 *vs.* 96 s). This trend continued for 0.5 A cm^{-2} and 0.2 A cm^{-2}.

The CO_2 breakthrough time increasing with decreasing current density is intuitive as the rate of ion movement through the AEM is slower at lower current density. The timescale for CO_2 breakthrough was much longer than the amount of time it would take for an ion to travel between the cathode and anode. At current densities of 2.0 A cm^{-2}, 1.0 A cm^{-2}, 0.5 A cm^{-2}, and 0.2 A cm^{-2}, the average time for a net single-charged anion to travel through the AEM is 410 ms, 820 ms, 1.6 s and 4.1 s, respectively (the ETFE-BTMA AEM had an IEC of 2.05 ± 0.05 mmol g^{-1} with *ca.* 43 μmol of charge-carrying, covalently-bound positively-charged groups in the 5 cm^2 membrane active area). The fact that the breakthrough time for CO_2 was much longer than the average time it takes for an anion to move from the cathode to the anode directly supports the idea that CO_2 is not emitted as part of a direct electrochemical process during normal operation and needs time to reach a critical concentration in the anode that allows it to be released into the anode exhaust (through the equilibrium reactions of Equations 2-3). This explains the lag in the CO_2 release as well as provides an explanation as to why breakthrough occurs earlier at higher currents since CO_3^{2-} back-diffusion is less effective – resulting in critical anode concentrations being reached sooner. At steady-state, the rate of CO_3^{2-} formation at the cathode will equal the rate of carbonate release (CO_2 emission) at the anode; the transient and steady-state fluxes for CO_3^{2-} reaction and CO_2 emission at several current densities and CO_2 concentrations to the cathode are given in Figure 2c.

From the transient flux data, the amount of carbonate in the system at steady-state, as well as the degree of carbonation, could be calculated (Table S1 and subsequent discussion in the Supporting Information). As expected, there was a greater amount of CO_3^{2-} present in the system with higher concentrations of CO_2 in the cathode stream. It was also found that the total amount of CO_3^{2-} in the system decreased with increasing current density. The change in the total number of CO_3^{2-} anions in the system with current density and cathode CO_2 concentration clearly explains the trends in the ASR. However, one interesting observation was that a plot of the total carbonate in the system vs. the change in the ASR, Figure 3, did not yield a single straight line for all conditions, but there were trends as a function of current density and CO_2 concentration. To understand this, it should be noted that the high frequency resistance measurement by the fuel cell test station is only measuring the two closest points separated by the ionomer; in other words, it is essentially a measurement of the membrane resistance. Therefore, the fact that the ASR is lower at a higher current density, even under conditions where the total amount of CO_3^{2-} in the cell is nearly identical to a lower current density, suggests that there is less carbonate in the AEM and more carbonate in the anode electrode as the current density is increased.

In summary, there were seven interesting observations when CO_2 was fed to the AEMFC cathode: 1) the CO_2 concentration leaving the cathode was only very modestly affected by the current density (Figure 2b), at least at the high flowrates investigated in this work; 2) the decrease in the cell voltage (Figure 2a) started to occur before CO_2 was measured in the anode exhaust; 3) the ASR increased immediately when CO_2 was added to the cell (Figure 2a); 4) the steady-state ASR was realized before the steady-state voltage was achieved and CO_2 was measured in the anode effluent (Figure 2a and 2b); 5) the steady-state ASR increased with decreasing current density (Figure 2a); 6) increasing current density decreased the amount of CO_3^{2-} present in the system at steady-state (Table S1); and 7) even at the highest current density and lowest CO_2 concentration (2.0 A cm^{-2} and 100 ppm, respectively) the CO_2-related overpotential was significant (167 mV), and the CO_2-related overpotential at 2.0 A cm^{-2} and pseudo-air conditions (400 ppm CO_2) was even higher (259 mV). Combined, these observations suggest that: i) CO_3^{2-} formation at the cathode is very rapid (likely in quasi-equilibrium, which will be discussed more later); ii) initially CO_3^{2-} accumulates in the membrane and anode electrode and release is slow until a critical concentration is reached; and iii) higher current densities increase the amount of CO_3^{2-} in the anode electrode.

To further study the dynamics of CO_2 uptake and CO_3^{2-} formation in the AEMFC system, as well as to simulate CO_2 that would build up in the anode or could be formed as an oxidative product of an alcohol fuel, CO_2 was also directly fed to the anode. For comparison sake, the CO_2 concentration in the anode H_2 reacting gas was also 400 ppm. The results of these experiments are shown in Figures 2d-2f. The first thing that should be noted is that while current was flowing,

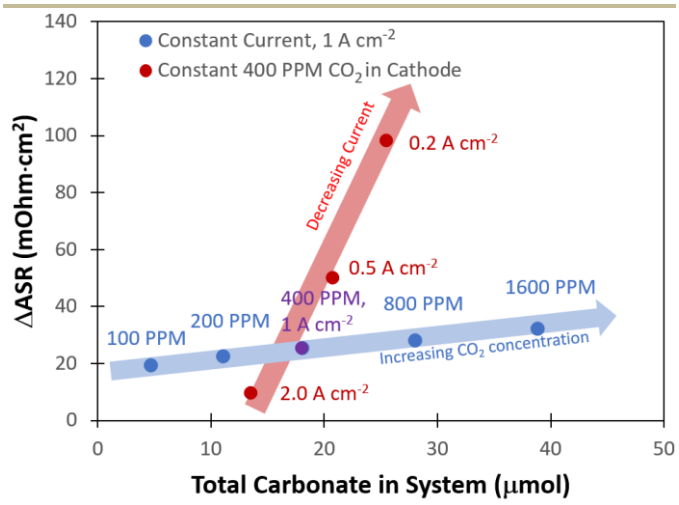

Fig. 3. ASR changes vs. quantity of carbonate in the cell as a function of current density and cathode CO_2 concentration. The fact that the relationship between the amount of carbonate and the change in the ASR does not fall on a single line suggests that more of the carbonates are in the anode electrode than the AEM with increasing current density.

no measurable CO_2 was ever found leaving the cathode, which can be attributed to the high net anionic flux relative to typical diffusion rates. Simply, CO_3^{2-} cannot diffuse and accumulate to a critical concentration at the cathode faster than migration pushes it to the anode under the conditions tested. Therefore, Figure 2e only shows the CO_2 concentration of the anode effluent and Figure 2f only shows the anode CO_2 flux. Like the cathode, there was approximately a 45 s lag between the time that CO_2 was turned on and its measurement (Figure S3, Supporting Information file). In this set of experiments, the dynamic CO_2 concentration in the effluent (before steady-state) increased with increasing current density, suggesting lower CO_2 uptake and CO_3^{2-} formation at higher currents. Also, the overall voltage decrease and ASR increase were both lower (but only slightly so) when CO_2 was fed to the anode *vs.* the cathode, most likely because of reduced carbonation stemming from the direction of ion transport.

Relationship Between Anode-Evolved CO_2 and the CO_2 Concentration in the Cathode

At practical fuel cell current densities, the vast majority of the charge is carried by OH^-, not CO_3^{2-}, even at very high levels of carbonation. Therefore, a metric relating the amount of charge carried by CO_3^{2-} (measured by the flux of CO_2 leaving the anode) at various current densities and CO_2 levels in the cathode (e^-/CO_2) would be useful – not only for fuel cells, but also for potential applications such as AEM-based electrochemical CO_2 capture [39]. Relating this ratio to the partial pressure of CO_2 in the cathode starts by defining the metric:

$$\log\left(\frac{e^-}{CO_2}\right) = log\left(\frac{i}{i_c}\right) = \log i - \log i_c \qquad (7)$$

where i is the total current and i_c is the component of the total charge carried by CO_3^{2-}. This is an acceptable definition because at steady-state, when the net accumulation of CO_2/CO_3^{2-} in the membrane is zero, the amount of CO_3^{2-} formed in the cathode and carried through the AEM by is balanced by current through the external circuit. An expression for i_c can be obtained by assuming Butler-Volmer-type kinetics (assuming that the ORR at the cathode, where the CO_3^{2-} is formed, is irreversible), and correcting the directionality of the current:

$$i_c = -i_o exp\left[\frac{-\alpha F}{RT}\left(E - E^{o'}\right)\right] \qquad (8)$$

where i_o is the exchange current density, α is the effective transfer coefficient, F is Faraday's constant, R is the ideal gas constant, E is the electrode potential and $E^{o'}$ is the formal potential. Rearranging:

$$E - E^{o'} = \frac{RT}{\alpha F} ln\, i_o - \frac{RT}{\alpha F}\ln i_c = \frac{2.303RT}{\alpha F} log\, i_c - \frac{2.303RT}{\alpha F}\log i_o \qquad (9)$$

It has been noted in the literature [15], and suggested by the data in Figure 2, that carbonation during the ORR is very fast, and, therefore, it can be assumed that the CO_2 in the cathode gas stream is always in quasi-equilibrium with the generated anions. This Nernstian process can be represented by the Nernst equation, combining the reactions in Equations 1 and 2, where the equilibrium potential is replaced by the actual electrode potential:

$$E - E^{o'} = \frac{RT}{nF}\ln\frac{P_{O2}P_{H2O}^2P_{CO2}^4}{[HCO_3^-]^4} = \frac{2.303RT}{nF}\log\frac{P_{O2}P_{H2O}^2}{[HCO_3^-]^4} + \frac{2.303RT}{nF}\log P_{CO2}^4 \qquad (10)$$

where P_i is the partial pressure of each gas, $[HCO_3^-]$ is the concentration of HCO_3^- in the AEM, and n is the number of electrons transferred in the ORR (n=4). It has been shown [16] and is generally accepted in the field (and assumed above) that the dominant anion in the operating AEMFC is CO_3^{2-}, not HCO_3^-. Therefore, it is important to express the Nernstian process relative to CO_3^{2-}, not HCO_3^-. Inserting the equilibrium expression between the CO_3^{2-} and HCO_3^- (Equation 11) into Equation 10:

$$[HCO_3^-] = \frac{[CO_3^{2-}]P_{H2O}}{[OH^-]K_{b2}} \qquad (11)$$

$$E - E^{o'} = \frac{RT}{nF}\ln\frac{P_{O2}P_{CO2}^4[OH^-]^4K_{b2}^4}{P_{H2O}^2[CO_3^{2-}]^4} = \frac{2.303RT}{nF}\log\frac{P_{O2}[OH^-]^4K_{b2}^4}{P_{H2O}^2[CO_3^{2-}]^4} + \frac{2.303RT}{nF}\log P_{CO2}^4 \qquad (12)$$

where $[CO_3^{2-}]$ is the concentration of carbonate in the AEM and K_{b2} is the equilibrium constant for the reaction in Equation 3. Combining Equations 9 and 12, i_c can be found as a function of the partial pressure of CO_2 in the cathode.

$$log\, i_c = \log i_o - \frac{\alpha}{n}\log\frac{P_{O2}[OH^-]^4K_{b2}^4}{P_{H2O}^2[CO_3^{2-}]^4} + \alpha\log P_{CO2} \qquad (13)$$

This result suggests that the CO_3^{2-} current should increase with the partial pressure of CO_2 in the cathode, which is logical. The final step in the derivation, relating the number of electrons transferred to the CO_2 partial pressure, combines equations 7 and 13.

$$\log\left(\frac{e^-}{CO_2}\right) = \left[\log i - \log i_o + \frac{\alpha}{n}\log\frac{P_{O2}[OH^-]^4K_{b2}^4}{P_{H2O}^2[CO_3^{2-}]^4}\right] - \alpha\log P_{CO2} \qquad (14)$$

Equation 14 makes two predictions, both of which are confirmed experimentally in Figure 4, which shows the results of steady-state measurements of CO_2 emission at various current densities and

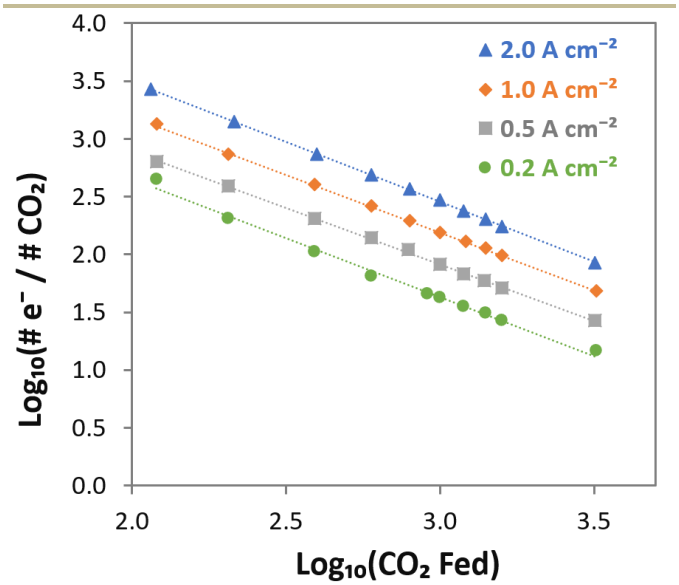

Fig. 4. Visualizing the steady-state transport of CO_2/CO_3^{2-} from the cathode to the anode in AEMFCs operating at 0.2, 0.5, 1 and 2 A cm^{-2} at 60°C over a wide range of CO_2 concentrations. The linear relationship with a slope of -1 verifies the relationship predicted in Equation 14 between the cathode CO_2 feed concentration and the portion of the charge that is carried by CO_3^{2-}, showing that CO_2 uptake and CO_3^{2-} incorporation is a Nernstian process and driven by the ORR.

concentrations. First, at any one current density (where everything in the brackets in Equation 14 is constant), there is a linear relationship between the log e^-/CO_2 and log P_{CO2} with a negative slope equal to the effective ORR transfer coefficient. The slope in Figure 4 is approximately -1, which is consistent with measurements of the effective transfer coefficient for the ORR in operating fuel cells [40,41]. Second, this equation predicts that lines at other current densities should be parallel as long as the mechanism is unchanged, and that higher current densities will yield a lower portion of CO_3^{2-} carrying the charge (increasing log e^-/CO_2). In fact, Figure 4 shows that charge is overwhelmingly carried by OH^- in these systems – even when the degree of carbonation at steady-state (Table S1 in the Supporting Information) is high. Only at very high CO_2 concentrations (3200 ppm) and low operating current densities (0.2 A cm^{-2}) is the portion of the charge carried by the CO_3^{2-} ion significant (*ca.* 10%), though these are not realistic operating conditions for AEMFCs (whereas 400 ppm is). However, the fact that carbonate does carry charge through the system when CO_2 is present has significant impacts on the operating voltage, which will be discussed later.

The results from Figure 2, Figure 4 and Table S1 show that the large overpotentials experienced by AEMFCs when CO_2 is added to the inlet streams are caused by a relatively small overall CO_3^{2-} population. What is missing from the literature, and the discussion thus far, is a conclusive determination of which of the fundamental drivers (Ohmic, Nernstian or anode HOR kinetics) primarily control the carbonate-related losses. Such insight would be invaluable in understanding the behavior (and design) of ambient air-utilizing AEMFC systems.

Deconvolution of Carbonate-Related Losses in Operating AEMFCs

Though the previous two sections have established some basic parameters for the behavior of CO_3^{2-} in operating AEMFCs (*e.g.* it induces polarization losses, is formed in quasi-steady-state with the ORR and its concentration gradient changes with feed concentration and current density), what would be the most helpful from a design and operation perspective is a quantitative deconvolution of the polarization losses. Identifying which of the carbonate-related processes is performance-limiting would allow for solutions to be proposed and evaluated systematically.

The first step in quantifying the carbonate-related losses in operating AEMFCs was to track the performance decline for cells operating at steady-state at several current densities over a wide range of cathode CO_2 concentrations. The response of a steady-state AEMFC operating at 1 A cm^{-2} to the introduction of 100, 200, 400, 800, 1600, and 3200 ppm CO_2 to the cathode reacting gas is shown in Figure 5a, and equivalent data for AEMFCs operating at 0.2, 0.5 and 2.0 A cm^{-2} are provided in Figures S9a – S9c in the Supporting Information file. Between each tested CO_2 concentration, the cell was rapidly decarbonated as described in the Experimental section. The data shown in Figures 5a and S9a – S9c show one hour of AEMFC behavior at each CO_2 concentration – the first 30 min segment shows the carbonation event and the re-establishment of a new steady-state. The second 30 min segment shows the initial response following CO_2 removal (where pure O_2 is again fed).

As discussed earlier, the introduction of CO_2 to operating AEMFCs initiates an interesting series of dynamic events that, in concert, lead to reduced steady-state performance through three mechanisms: increasing the Ohmic resistance (*ΔASR*), increasing the

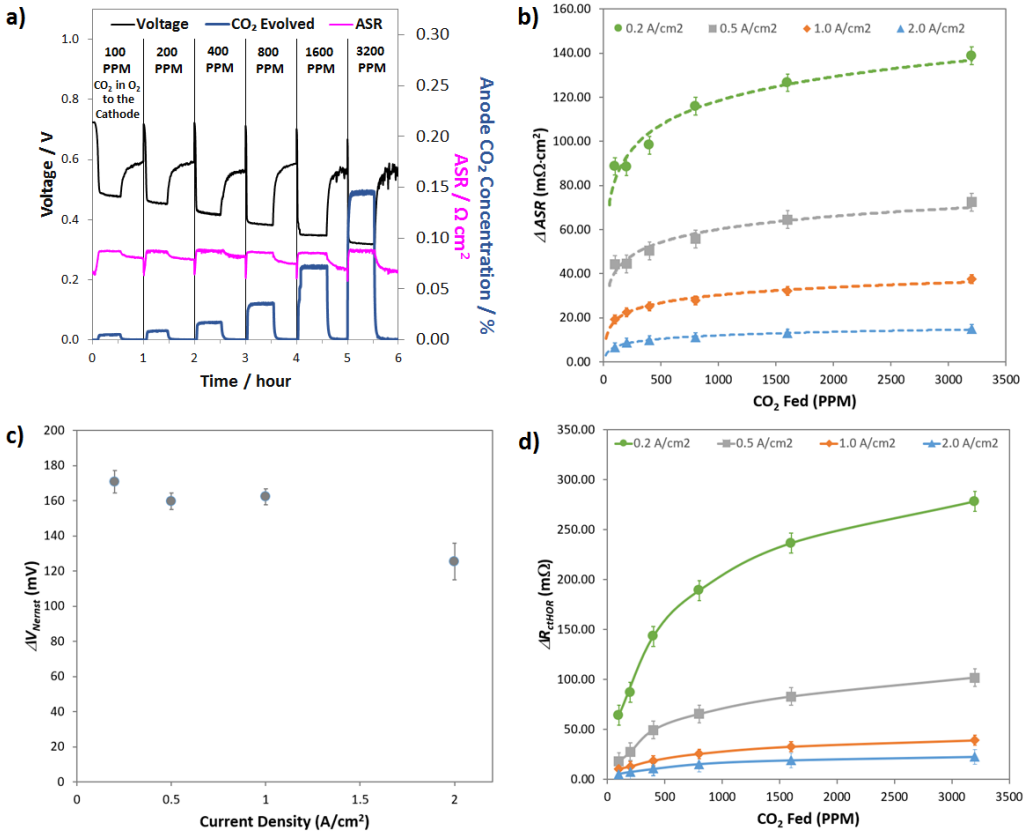

Fig. 5. a) Response of an AEMFC operating at 1.0 A cm^{-2} to various concentrations of CO_2 in the cathode reacting gas; b) Summary of the change in the ASR at various current densities and CO_2 concentrations; c) AEMFC Nernstian voltage loss as a function of current density; d) Increase in anode charge transfer resistance with increasing CO_2 concentration and decreasing current density. All cells were operated at 60°C with an ETFE-BTMA AEM (IEC = 2.05 ± 0.05 mmol g^{-1}).

anode charge transfer resistance (ΔR_{ctHOR}) and increasing the thermodynamic anode potential (ΔV_{Nernst}). The challenge here is to find a systematic way to use the CO_2 exposure and removal data in Figure 5a (Figure S9 in the Supporting Information file) to quantify the contribution of each of these resistances to the total CO_2-related overpotential. The general approach to extracting these three losses from the data was consistent regardless of the experiment. A representative description for 400 ppm CO_2 at 1.0 A cm^{-2} is given here for illustrative purposes, and then the summary of all of the calculated parameters is shown in Figures 5b – 5d.

Before adding any CO_2 to the AEMFC operating at 1.0 A cm^{-2}, steady-state performance was established. The steady-state operating voltage at this condition was 0.72 V. The operating voltage for this cell is given by Equation 4. What this means is that the CO_2-free steady-state operating voltage already contains $R_{\Omega,OH}$, R_{ctORR} and R_{mtORR}; hence, the deviation of the operating voltage after adding CO_2 will only come from ΔV_{Nernst}, ΔASR and ΔR_{ctHOR}, as shown in Equation 6. After adding 400 ppm CO_2 to the cell, the new steady-state voltage that was reached was 0.44 V – meaning that the total CO_2-related overpotential was *ca.* 280 mV. While the stoichiometries used in these experiments were high, leading to high CO_2 dosages, the observed performance losses (in combination with the total CO_2-related overpotential of ~260 mV for a cell operating at 2.0 A cm^{-2} with 400 ppm CO_2) suggest that the "self-purging" mechanism has a relatively modest effect in decarbonating the cell, and reducing CO_2-related voltage losses to an acceptable level during operation on direct ambient air will be a significant challenge, and may not be possible at all.

The first CO_2-related loss that was calculated was ΔASR. The ASR as a function of time is shown in Figure 5a, and under this operating condition, ΔASR was 25 mΩ cm^2. Assuming this ΔASR resulted in proportional Ohmic losses, at 1 A/cm^2 this would result in an Ohmic loss of 25 mV. For completeness, we acknowledge that the measured ASR values do not yield the exact potential drop related to ion movement through the AEM due to the influence of diffusion [31,32]. However, the value measured here does give an accurate measure of average anion mobility and is presented here as an overestimation of the maximum Ohmic resistance that could be attributed to carbonation. Perhaps what is most important is that this observation clearly shows that the ASR change caused by the emergence and transport of CO_3^{2-} through the AEM represents a very small portion of the overall CO_2-related overpotential (<10%).

For the AEMFC operating at 1.0 A cm^{-2} with 400 ppm CO_2 in the cathode, at minimum, 255 mV of the CO_2-related loss remains to be accounted for. The next stage of the deconvolution comes when CO_2 is removed from the cathode stream. Experimentally, a rapid increase in the cell potential was observed, to *ca.* 0.54 V, though the potential never exactly levels off to reach a new steady-state. That is because the only way that a true steady-state can be reestablished is for all of the CO_3^{2-} to be removed, either by waiting for many hours (Figure S1), or by accelerated decarbonation at 0.1 V (Figure S2). However, it is important to consider what is happening phenomenologically in the AEMFC when the cathode gas is switched from CO_2-containing O_2 to pure O_2. When CO_2 is removed from the cathode, no new CO_3^{2-} anions are generated there and the concentration of CO_3^{2-} at that electrode drops towards zero. As OH^- is produced, the CO_3^{2-} that was in the cathode and the AEM is progressively pushed toward the anode by migration (recall that the migrational residence time through the AEM at this current is 820 ms). This suggests that there will be a brief transient period to establish a new quasi steady-state (on the order of ~10 min according to Figure 5a) after which essentially all of the migrational charge that is carried from the cathode to the anode is carried by OH^-. If this is the case, at the new quasi steady-state, no OH^- will need to be provided by diffusion in the anode for the HOR to occur. Therefore, the voltage increase during this 10 min establishment of the new quasi steady-state after CO_2 is removed can be mostly attributed to the relaxation of the kinetic limitations described by ΔR_{ctHOR} (though the new ASR acting on charge transport needs to be corrected for as well). At the condition above, 1.0 A cm^{-2} with 400 ppm CO_2 fed to the cathode, ΔR_{ctHOR} was calculated by Equations 15 and 16.

$$\Delta V_{ctHOR}(\mathrm{mV}) = [0.544\ \mathrm{V} - 0.443\ \mathrm{V}] \times 1000 - (1.0\ \mathrm{A\ cm^{-2}})(83.5\ \mathrm{m\Omega\ cm^2} - 75.3\ \mathrm{m\Omega\ cm^2}) = 93.7\ \mathrm{mV} \quad (15)$$

$$\Delta R_{ctHOR}(\mathrm{m\Omega}) = \frac{93.7\ \mathrm{mV}}{(1.0\ \mathrm{A\ cm^{-2}})(5\ \mathrm{cm^2})} = 18.7\ \mathrm{m\Omega} \quad (16)$$

Because not all of the reacting catalyst in the anode can be assumed to be completely void of carbonation effects (because of the balance of carbonate migration and diffusion), the calculations made from Equations 15 and 16 are likely a lower limit for ΔR_{ctHOR}, though the real value should be close since the rate of carbonate removal after the initial voltage increase is slow.

From here, the Nernst-related loss can be calculated for this case: 162 mV (281 mV - 25mV - 94 mV = 162 mV). Because the estimate for ΔR_{ctHOR} is a lower bound, 162 mV is an upper bound for the for ΔV_{Nernst}, though it should be close to the true value for the reasons discussed above. Interestingly, the Nernstian and charge-transport losses had a similar effect on the cell performance, and both were far more important in dictating the performance decline than the Ohmic loss.

Conducting the same analysis over the entire range of current densities and CO_2 concentrations can yield values for the total CO_2-related overpotential, ΔASR, ΔR_{ctHOR}, and ΔV_{Nernst} as well as the Ohmic voltage loss (ΔV_{Ohmic}) and the CO_2-related kinetic polarization (ΔV_{ctHOR}) at every condition. All of these values are given in Table S2 of the Supporting Information file. Performing the data deconvolution over such a wide range of current densities and cathode CO_2 concentrations yielded some very revealing trends and important insight into the behavior of carbonated AEMFCs. Not too surprisingly, the total CO_2-related overpotential was increased with decreasing current density and increasing CO_2 concentration in the cathode (Table S2 in the Supporting Information file). However, understanding why this happened requires digging into the trends in ΔASR, ΔR_{ctHOR}, and ΔV_{Nernst} more extensively.

Figure 5b presents the ΔASR values at all conditions. As the concentration of CO_2 in the cathode reacting gas was decreased, there less of a negative impact on the ASR. This makes sense from the transient and steady-state experimental results (Table S1, Supporting Information), which showed that the total amount of CO_3^{2-} in the AEMFC was lower at lower cathode CO_2 concentration and increased current density. As discussed earlier, the overall trends in the ASR with current density and cathode CO_2 concentration (Figure 3) led to the conclusion that increasing the current density shifts the CO_3^{2-} concentration gradient toward the anode electrode. Hence, with increasing current density, relatively less and less CO_3^{2-} is present in the AEM (though the total CO_3^{2-} flux is higher, Figure 2c), resulting in a lower ASR.

The fact that the concentration gradient shifts toward the anode with current density might lead to the assumption that ΔV_{Nernst} (Figure 5c) should also increase with current density. However, there are two counter points that require discussion. First, the total quantity of carbonate in the cell is decreasing with increasing current

density, which alone might limit the achievable value for ΔV_{Nernst}, particularly at high currents. Second, the anode potential is measured at the outermost portion of the anode at the gas diffusion layer, which is likely the point of the highest CO_3^{2-} concentration, as illustrated in Figure 1, and it is possible for that one specific location to be close to saturation over a wide range of conditions. We observed that ΔV_{Nernst} appeared to decrease with increasing current density, though the values at current densities ≤ 1.0 A cm^{-2} were very similar.

The assertion that the outermost portion of the anode can be close to saturation was supported by the magnitude of ΔV_{Nernst} at the lower current densities, ~165 mV. The effective alkalinity of an AEMFC cathode is between pH 13 – 14. It is also known that CO_3^{2-} is overwhelmingly the dominant carbon-based charge carrier and this can only happen in water at pH values > 11. Therefore, the maximum pH shift that could be expected at the anode in an operating cell would be 3, resulting in a $\Delta V_{Nernst,max}$ of ca. 180 mV. The only data point in Figure 5c where ΔV_{Nernst} is markedly lower is at very high current, 2.0 A cm^{-2}, where ΔV_{Nernst} is ~125 mV. This lower value can be explained by either the lower overall carbonate concentration in the cell and anode at higher currents, and/or the development of a mixed potential throughout the anode because at high current density there is a significant number of OH^- ions being released throughout the anode as CO_2 is evolved through the reverse of Equations 2-3, though the root cause for this behavior will likely need to be teased out through computational modeling. It is also noteworthy that ΔV_{Nernst} was essentially unaffected by the cathode CO_2 concentration, which gives additional support to the arguments above. One area where the higher carbonate concentration in the anode did have a major impact on the AEMFC behavior is ΔR_{ctHOR}, Figure 5d. At higher overall carbonate content (increased cathode CO_2 concentration and/or lower current density) ΔR_{ctHOR} was also higher, and the current density had a particularly profound influence on the effect of the cathode CO_2 concentration. This observation yields important insight into the location of carbonate in electrodes, suggesting that higher current densities compress the volume occupied by carbonates to the outermost portion of the anode, which effectively allows more catalyst sites to have easy access to reacting OH^-.

AEMFC Response at Low CO_2 Concentrations

A practical interpretation of the experiments shown in Figure 5 is that the polarization losses from AEMFC carbonation are significant at all current densities and near-ambient CO_2 concentrations, and that AEMFCs will likely require pre-scrubbing of CO_2 from the operating air. Additionally, the dynamics of CO_2 uptake (fast) and release (slow) mean that even if CO_2 could be quickly removed from the anode stream to avoid significant accumulation, losses would still be high. One sensible approach to reducing CO_2-related overpotential is to lower the cathode inlet concentration, which is particularly intriguing for stationary implementations of AEMFCs where the volume and weight of a CO_2 scrubber is less of a concern than it is for mobile or transportation applications. Figure 6a explores the response of an AEMFC operating at 1 A cm^{-2} with 5 – 50 ppm CO_2 in the cathode reacting gas. Though the voltage loss was less than at higher concentrations, even down to 5 – 10 ppm CO_2 in the cathode, the CO_2-related polarization was significant, approximately 140 mV.

Figure 6b shows the response of an AEMFC operating at 1 A cm^{-2} with 5 – 50 ppm CO_2 added to the anode H_2 reacting gas. The behavior of low-level CO_2 in the anode is very similar to the cathode. At 10 ppm, the total CO_2-related voltage loss was 136 mV. For CO_2 present in both the cathode and anode, Figure 6 suggests that if there is a lower threshold below which an operating AEMFC is immune to carbonation, it is very low - below 5 ppm (although it should be noted that dosage is also important and decreasing flow rates could also have a beneficial impact).

Influence of Temperature on CO_2-Related Polarization Losses at 400 ppm

Figure 6 shows that removing even a large portion of the CO_2 in ambient air will not be sufficient to eliminate the CO_2-related losses in operating AEMFCs. In fact, we demonstrated that even at 5 ppm CO_2 significant performance losses occurred. Therefore, it is important for researchers to identify some fundamental and operational properties of the system that can be manipulated to reduce the AEMFC sensitivity to CO_2. One pathway to reducing the amount of carbonate accumulated in the system is to increase the cell operating temperature. Increasing temperature could possibly impact cell carbonation because: i) CO_2 has lower solubility in water as the temperature is increased;[42] ii) the kinetics for CO_2 release (reverse of Equations 2 and 3) at the anode will improve; iii) the mass

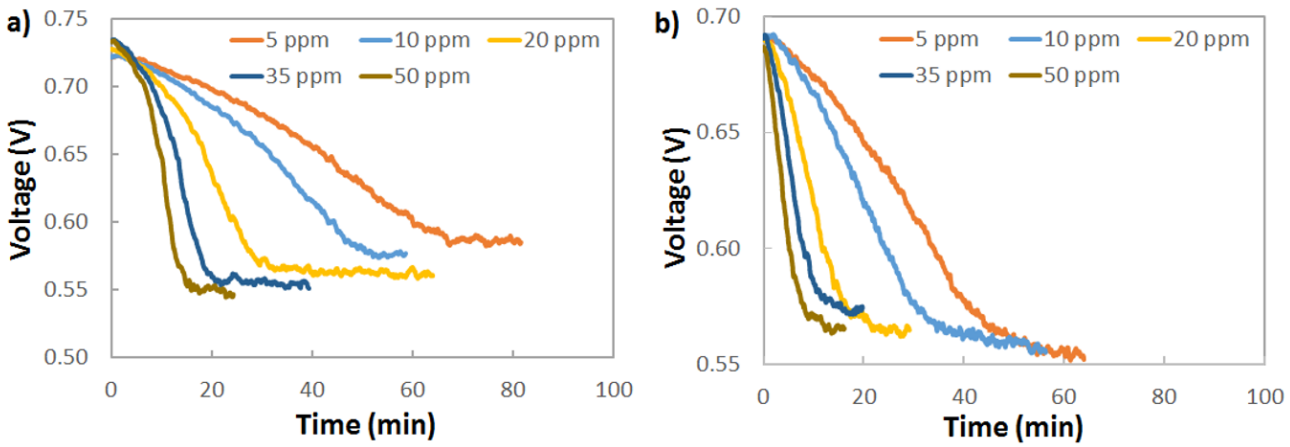

Fig. 6. Exploring the existence of a lower threshold concentration for CO_2 present in the a) cathode and b) anode compartments. The AEMFCs were operated at an operating current density of 1.0 A cm^{-2} at 60 °C with an ETFE-BTMA AEM.

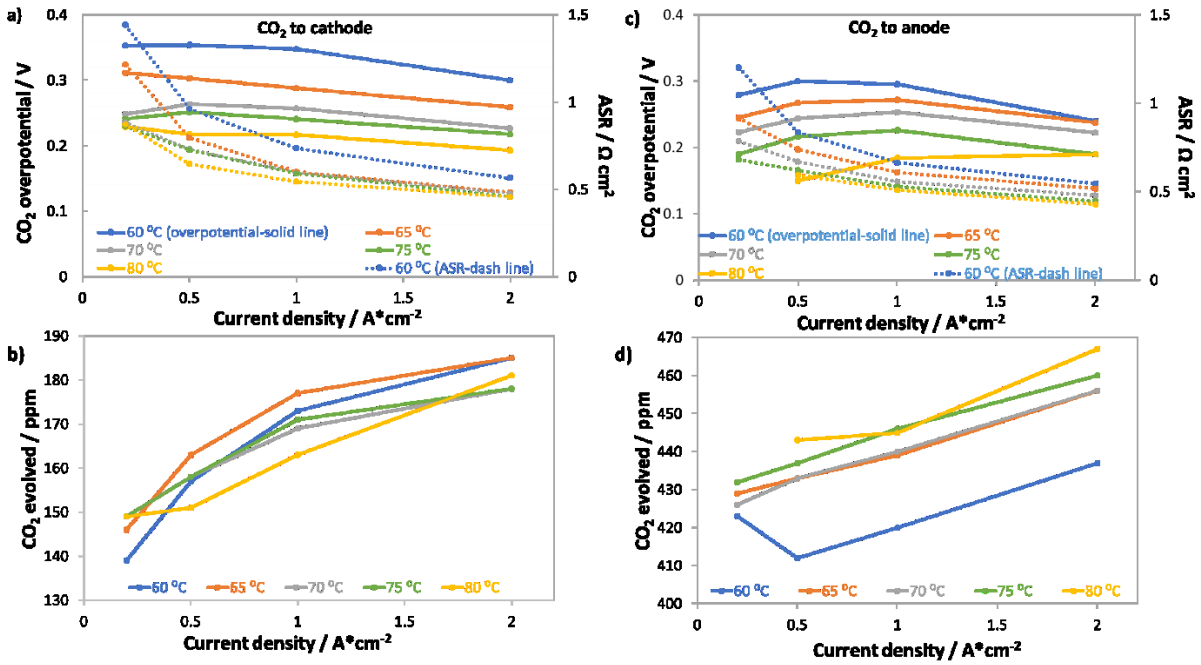

Fig. 7. Impact of temperature on the total CO_2-related overpotential, ASR and anode CO_2 exhaust with 400 ppm CO_2 fed to the cathode at multiple current densities. Total CO_2 overpotential (solid lines) and ASR (dashed lines) when CO_2 was fed to the a) cathode and c) anode. CO_2 concentration in the anode effluent when CO_2 was fed to the b) cathode and d) anode. An LDPE-BTMA AEM (IEC = 2.5 mmol g^{-1}) was used in these experiments

transport rate of evolved gaseous CO_2 from the anode will increase; and iv) the intrinsic kinetics for the ORR and HOR will improve.

Figures 7 summarizes the response of AEMFCs with a LDPE-BTMA membrane operating at 0.2, 0.5, 1.0 and 2.0 A cm^{-2} and several temperatures (60, 65, 70, 75, and 80 °C) following the introduction of 400 ppm CO_2 to the cathode or anode. Regardless of where the CO_2 was introduced, increasing the temperature simultaneously decreased the total CO_2 overpotential and the ASR (Figures 7a and 7c). This experimental result is in stark contrast to recent modeling results that suggested increasing the cell temperature would not have a beneficial effect on AEMFC operation [16]. Figure 7b shows that as the temperature was increased, the concentration of CO_2 being emitted from the anode side of the cell (when it is fed to the cathode) decreased. The most likely explanation for this trend, and coupled performance increase, is that less CO_2 was taken up into the system. Figure 7d shows that when CO_2 was fed to the anode, increasing the temperature resulted in lower CO_2 uptake at that electrode as well, which is shown by the increasing concentration of CO_2 in the anode effluent. It should also be noted in Figures 7b and 7d that the values trend upward with increasing current density due to the consumption of the fuel and oxidant gases. Positively, the improved performance at elevated temperatures suggests that increasing temperature is indeed one possible mechanism to improve the CO_2 tolerance of operating AEMFCs; however, the CO_2-related overpotential is still too high for many practical applications. A combination of lower CO_2 concentration, more modest air stoichiometry, and elevated temperature can further reduce the total CO_2 overpotential. For instance, we observed that an AEMFC operating at 1 A cm^{-2} and 80°C with 10 ppm CO_2 fed to the cathode (the same LDPE-BTMA membrane) had a total CO_2 overpotential of only 90 mV.

Deconvoluted data for AEMFCs operating at different temperatures but at a constant current of 1 A cm^{-2} and constant cathode CO_2 concentration of 400 ppm (showing the ΔASR, ΔV_{Nernst} and ΔR_{ctHOR}) can be found in Table S3 in the Supporting Information. As expected, the ASR generally decreased with increasing temperature due to the lower quantity of carbonates that were taken up into the membrane. However, the ASR value only varied slightly with increasing temperature, which meant that a similar portion of CO_3^{2-} anions were carrying the charge through the AEM (supported by the results of accelerated decarbonation experiments at 0.1 V, Table S4 in the Supporting Information), which led ΔR_{ctHOR} to be fairly constant with temperature as well. Therefore, the primary impact of an overall reduced number of CO_3^{2-} anions in the AEM was that the carbonate accumulation in the anode (and hence the concentration gradient across the cell) was less severe with increased temperature. As a result, ΔV_{Nernst} was the most dependent on temperature, decreasing by nearly 50% from 60 – 80 °C.

It is possible that even higher temperatures (> 90 °C) may help. Though no AEMs are currently readily available with stability above 80 °C in highly alkaline media that also have acceptable conductivity and water transport properties [3], there is promising work ongoing in this area. Recent reports by Yan and coworkers [3,43] have shown that it is possible to create AEMs that are conductive and stable to at least 95 °C. Another important consideration for AEM and AEMFC researchers is that the membrane chemistry (both backbone and headgroup) and morphology are likely to influence the uptake, transport and release of CO_2. What this really points to is that improving the CO_2 tolerance of AEMFCs will likely require a combination of approaches to achieve success, at least some of which are not known today and will be particularly challenging for dynamic operation.

Conclusions

Even in highly performing AEMFCs, the addition of CO_2 has a severe negative impact, where the cell operating voltage is generally decreased by 200 – 400 mV depending on the reaction conditions. Lower CO_2 concentration in the reacting gas, higher current density and higher operating temperature all reduce the voltage penalty, but none have been shown be able to sufficiently minimize the CO_2 impact. One of the primary reasons for this is that decarbonation of the cell does not occur through direct electrochemical reaction. This means that decarbonation during operation by the so-called "self-purging" mechanism is slow, taking several hours even after only transient exposure to CO_2. Hence, "self-purging" cannot be relied upon to decarbonate a real system efficiently.

The dominating loss in operating AEMFCs in the presence of CO_2 is not due to an increase in the Ohmic resistance from electrolyte carbonation. The dominating mechanism for voltage loss is accumulation of carbonate anions in the anode, which results in two performance-robbing mechanisms: 1) a Nernstian thermodynamic shift in the anode potential from a decrease in the anode pH with carbonates; and 2) an increase in charge transfer resistance due to a lack of availability of reacting OH^- anions. The CO_2 concentration in the cathode and the current density are both determining factors for the quantity of CO_3^{2-} in the system, and the current density appears to play a primary role in dictating the CO_3^{2-} location and distribution. The HOR charge transfer resistance increases markedly with both increased CO_2 concentration and lower current density. Increasing the cell operating temperature appears to have almost no effect on the charge transfer resistance, but a significant effect on the Nernstian loss, meaning that the total CO_2-related overpotential can be reduced by increasing the temperature – or better yet, through a combination of higher current density, lower CO_2 concentration and higher operating temperature.

These new insights can help both modeling groups and experimental researchers to better understand operating AEMFCs, as well as allow them to pose and assess new solutions.

Conflicts of interest

There are no conflicts to declare.

Acknowledgements

USC gratefully acknowledges the financial support of the U.S. National Science Foundation (Award Number: 1803189) for the effort expended by Y.Z., T.J.O. and W.E.M. to perform the AEMFC experiments, analyze data and prepare the manuscript. The AEM and AEI materials were synthesized using resources funded by the UK's Engineering and Physical Sciences Research Council (grant EP/M014371/1). Funding for B.S.P. was provided by the U.S. Department of Energy Office of Energy Efficiency and Renewable Energy Fuel Cell Technologies Office. The views and opinions of the authors expressed herein do not necessarily state or reflect those of the United States Government or any agency thereof. Neither the United States Government nor any agency thereof, nor any of their employees, makes any warranty, expressed or implied, or assumes any legal liability or responsibility for the accuracy, completeness, or usefulness of any information, apparatus, product, or process disclosed, or represents that its use would not infringe privately owned rights. The U.S. Government retains and the publisher, by accepting the article for publication, acknowledges that the U.S. Government retains a nonexclusive, paid-up, irrevocable, worldwide license to publish or reproduce the published form of this work, or allow others to do so, for U.S. Government purposes.

References

1 B. P. Setzler, Z. Zhuang, J. A. Wittkopf and Y. Yan, *Nat. Nanotechnol.*, 2016, **11**, 1020–1025.

2 J. R. Varcoe, P. Atanassov, D. R. Dekel, A. M. Herring, M. A. Hickner, P. A. Kohl, A. R. Kucernak, W. E. Mustain, K. Nijmeijer, K. Scott, T. Xu and L. Zhuang, *Energy Environ. Sci.*, 2014, **7**, 3135–3191.

3 J. Wang, Y. Zhao, B. P. Setzler, S. Rojas-carbonell, C. Ben Yehuda, A. Amel, M. Page, L. Wang, K. Hu, L. Shi, S. Gottesfeld, B. Xu and Y. Yan, *Nat. Energy*, 2019, **4**, 392–398.

4 S. Gottesfeld, D. R. Dekel, M. Page, C. Bae, Y. Yan, P. Zelenay and Y. S. Kim, *J. Power Sources*, 2018, **375**, 170–184.

5 W. E. Mustain, *Curr. Opin. Electrochem.*, 2018, **12**, 233–239.

6 S. Maurya, S. Noh, I. Matanovic, E. J. Park, C. N. Villarrubia, U. Martinez, J. Han, C. Bae and Y. S. Kim, *Energy Environ. Sci.*, 2018, **11**, 3283–3291.

7 L. Wang, J. J. Brink, Y. Liu, A. M. Herring, J. Ponce-González, D. K. Whelligan and J. R. Varcoe, *Energy Environ. Sci.*, 2017, **10**, 2154–2167.

8 T. J. Omasta, L. Wang, X. Peng, C. A. Lewis, J. R. Varcoe and W. E. Mustain, *J. Power Sources*, 2018, **375**, 205–213.

9 T. J. Omasta, A. M. Park, J. M. Lamanna, Y. Zhang, X. Peng, L. Wang, D. L. Jacobson, J. R. Varcoe, D. S. Hussey, B. S. Pivovar and W. E. Mustain, *Energy Environ. Sci.*, 2018, **11**, 551–558.

10 G. Huang, M. Mandal, X. Peng, A. C. Yang-Neyerlin, B. S. Pivovar, W. E. Mustain and P. A. Kohl, *J. Electrochem. Soc.,*2019, **166**, In Press.

11 S. M. Alia, K. Neyerlin, K. Hurst, J. W. Zack, S. A. Mauger, W. W. McNeary, A. Weimer, W. Medlin, S. Zaccarine, C. Ngo, S. Pylypenko, K. Buechler and B. S. Pivovar, in *The Electrochemical Society Meeting Abstracts*, 2018, vol. 44, pp. 1505–1505.

12 S. M. Alia, S. Stariha, R. L. Borup and B. S. Pivovar, in *The Electrochemical Society Meeting Abstracts*, 2018, vol. 46, pp. 1604–1604.

13 W. E. Mustain, in *The Electrochemical Society Meeting Abstracts*, 2018, vol. 47, pp. 1637–1637.

14 T. J. Omasta, X. Peng and W. E. Mustain, in *The Electrochemical Society Meeting Abstracts*, 2018, vol. 30, pp. 1754–1754.

15 N. Ziv, W. E. Mustain and D. R. Dekel, *ChemSusChem*, 2018, **11**, 1136–1150.

16 U. Krewer, C. Weinzierl, N. Ziv and D. R. Dekel, *Electrochim. Acta*, 2018, **263**, 433–446.

17 M. R. Gerhardt, L. M. Pant, H.-S. Shiau and A. Z. Weber, *ECS Trans.*, 2018, **86**, 15–24.

18 S. D. Poynton, R. C. T. Slade, T. J. Omasta, W. E. Mustain, R. Escudero-Cid, P. Ocón and J. R. Varcoe, *J. Mater. Chem. A*, 2014, **2**, 5124–5130.

19 J. Ponce-Gonzalez, D. K. Whelligan, L. Wang, R. Bance-Soualhi, Y. Wang, Y. Peng, H. Peng, D. C. Apperley, H. N. Sarode, T. P. Pandey, A. G. Divekar, S. Seifert, A. M. Herring, L. Zhuang and J. R. Varcoe, *Energy Environ. Sci.*, 2016, **9**, 3724–3735.

20 R. Zeng, S. D. Poynton, J. P. Kizewski, R. C. T. Slade and J. R. Varcoe, *Electrochem. commun.*, 2010, **12**, 823–825.

21 A. Amel, N. Gavish, L. Zhu, D. R. Dekel, M. A. Hickner and Y. Ein-Eli, *J. Memb. Sci.*, 2016, **514**, 125–134.

22 T. P. Pandey, A. M. Maes, H. N. Sarode, B. D. Peters, S. Lavina, K. Vezzù, Y. Yang, S. D. Poynton, J. R. Varcoe, S. Seifert, M. W. Liberatore, V. Di Noto and A. M. Herring, *Phys. Chem. Chem. Phys.*, 2015, **17**, 4367–4378.

23 M. L. Disabb-Miller, Y. Zha, A. J. DeCarlo, M. Pawar, G. N. Tew and Michael A. Hickner, *Macromolecules*, 2013, **46**, 9279–9287.

24 Z. Siroma, S. Watanabe, K. Yasuda, K. Fukuta and H. Yanagi, *ECS Trans.*, 2010, **33**, 1935–1943.

25 J. A. Wrubel, A. A. Peracchio, B. N. Cassenti, T. D. Myles, K. N. Grew and W. K. S. Chiu, *J. Electrochem. Soc.*, 2017, **164**, F1063–F1073.

26 M. R. Gerhardt, L. M. Pant and A. Z. Weber, *J. Electrochem. Soc.*, 2019, **166**, F3180–F3192.

27 Y. Wang, L. Li, L. Hu, L. Zhuang, J. Lu and B. Xu, *Electrochem. commun.*, 2003, **5**, 662–666.

28 K. Fukuta, in *AMFC Workshop*, 2011.

29 J. A. Vega, S. Smith and W. E. Mustain, *J. Electrochem. Soc.*, 2011, **158**, B349–B354.

30 Y. Matsui, M. Saito, A. Tasaka and M. Inaba, *ECS Trans.*, 2010, **25**, 105–110.

31 T. A. Greszler, T. E. Moylan and H. A. Gasteiger, in *Handbook of Fuel Cells-Fundenmentals, Technology and Applications*, 2009, vol. 6, pp. 729–748.

32 T. Greszler, T. Moylan and H. Gasteiger, in *The Electrochemical Society Meeting Abstracts*, 2008, vol. 11, pp. 955–955.

33 B. Kienitz, B. Pivovar, T. Zawodzinski and F. H. Garzon, *J. Electrochem. Soc.*, 2011, **158**, B1175–B1183.

34 B. Kienitz, Case Western Reserve University, 2009.

35 Y. A. Gomez, A. Oyarce, G. Lindbergh and C. Lagergren, *J. Electrochem. Soc.*, 2018, **165**, F189–F197.

36 M. Inaba, Y. Matsui, M. Saito, A. Tasaka, K. Fukuta, S. Watanabe and H. Yanagi, *Electrochemistry*, 2011, **5**, 322–325.

37 H. Yanagi and K. Fukuta, *ECS Trans.*, 2008, **16**, 257–262.

38 A. G. Divekar, B. S. Pivovar and A. M. Herring, *ECS Trans.*, 2018, **86**, 643–648.

39 W. A. Rigdon, T. J. Omasta, C. Lewis, M. A. Hickner, J. R. Varcoe, J. N. Renner, K. E. Ayers and W. E. Mustain, *J. Electrochem. Energy Convers. Storage*, 2017, **14**, 1–8.

40 J. X. Wang, F. A. Uribe, T. E. Springer, J. Zhangc and R. R. Adzic, *Faraday Discuss.*, 2008, **140**, 347–362.

41 H. Xu, Y. Song, H. R. Kunz and J. M. Fenton, *J. Electrochem. Soc.*, 2005, **152**, A1828.

42 B. Pivovar, D. Ruddy, M. Sturgeon and H. Long, *FY 2013 Annu. Prog. Rep. DOE Hydrog. Fuel Cells Progr.*, 2013, v235–v237.

43 T. Wang, L. Shi, J. Wang, Y. Zhao, B. P. Setzler, S. Rojas-carbonell and Y. Yan, *J. Electrochem. Soc.*, 2019, **166**, F3305–F3310.